Proceedings of Montreal 2018
Global Power and Propulsion Forum
7th – 9th May, 2018

GPPS-NA-2018-0036

UNSTEADY FLOW IN A LABYRINTH SEAL

Lars Wein
Institute of Turbomachinery and Fluid Dynamics
Leibniz Universitaet Hannover
wein@tfd.uni-hannover.de
Hannover, 30167, Germany

J. R. Seume and F. Herbst
Institute of Turbomachinery and Fluid Dynamics
Leibniz Universitaet Hannover
Hannover, 30167, Germany

ABSTRACT

Unsteady flow phenomena in turbomachinery are a source of aerodynamic losses and can adversely affect the durability of an engine. Examples for such flows are the flow through the cavities of the turbine hub or shroud labyrinth and rim seal. The re-entering flow causes mixing losses with the main flow and increases incidence on the following stator. In order to increase the efficiency level of modern gas and steam turbines, an improved understanding of the interaction between the secondary and primary air system is required. Turbulence-resolving numerical methods can provide such insights if the computational domain captures all dominant scales of the flow in time and space. For turbine rim seals, various experimental and numerical studies in the literature report the presence of large scale cavity modes with a periodicity of up to 120° *in the circumferential direction. For turbine shroud cavities such modes have not yet been observed.*

In this paper the time-resolved flow in the cavities of a stepped labyrinth seal is investigated. The aim is to identify the largest scales of the flow which determines the required size of the computational domain for scale-resolving simulations. A small CFD domain of 1° *circumferential extent leads to an incorrect prediction of the frequencies associated to leakage pulsation. This domain cannot resolve the largest scales present in full annulus CFD models. The largest scales, referred to as lobes, have a periodicity of* 12° *in the circumferential direction. As experimentally shown for turbine rim seals, these lobes are moving in the direction of rotation with* $0.76\Omega_{Rotor}$*. The frequency of leakage pulsation is higher then the frequency of the lobes and its dependence on the periodic boundary conditions is weaker. Furthermore, the presence and the frequency of the lobes depends on the seal pressure ratio and the pre-swirl of the flow.*

NOMENCLATURE

C_W	Dimensionless cooling flow rate
$F2$	SST-Blending Function
H	Channel height in mm
K	Swirl ratio
MP_i	Measurement plane i $= A$ and i $= B$
N	Rotational Speed in min^{-1}
P_i	LDV measurement points $i = 1 \ldots 9$
R	Rotor radius in mm
S	Vorticity in 1/s
St	Strouhal-Number
U	Circumferential velocity of the rotor in m/s
V	Absolute velocity of the fluid in m/s
Re_{ax}	Axial Reynolds-Number
c	Clearance height in mm
f	Frequency in Hz
h	Seal blade height in mm
k	Turbulence kinetic energy
l	Cavity length and blade spacing in mm
l_{vK}	von Karman length scale
$\dot{m}$	Mass flow rate in kg/s
n	Number of sealing fins
v_θ	Circumferential velocity of the fluid m/s
x_i^+	Non-dimensional wall distance
u_τ	Shear velocity in m/s

Greek Letters

Δ	Nodal distance in x, y and z
Ω	Angular velocity in 1/s
ω	Turbulent production rate
π	Total to static pressure ratio
δ_b	Boundary layer thickness in m
ν	Kinematic viscosity in m^2/s
ν_t	Eddy viscosity in m^2/s

INTRODUCTION

Modern axial compressors and turbines have already reached high efficiency levels, and according to Cumpsty [1] no major improvements are expected unless unsteady aerodynamics are considered in the design cycle. This requires extensive time-resolved numerical simulations and experimental measurements during research and development. One source of unsteady flow related losses in turbomachinery is the interaction of the secondary flow system with the main flow. For example, the interaction of the cavity flow re-entering the main flow path after flowing through the labyrinth seal of a shrouded rotor introduces mixing losses and increased incidence of the downstream stator [2]. This interaction is highly unsteady, and influenced by the rotor and stator potential fields. In order to reduce aerodynamic losses associated to the shroud cavity leakage, the physical mechanisms involved need to be investigated. This requires an accurate and time-resolved prediction or measurement of the main flow, the cavity flow and the mixing process. All three parts are challenging by themselves. As it can be seen in Henke et al. [3], Giboni et al. [4], and multiple others, this is not the case yet. However, it is not clear if the poor prediction is caused by the prediction of the cavity flow, the main flow, or the mixing process. Therefore, the single processes need to be investigated separately. The focus of this work is the cavity flow.

Unsteady flow features in turbomachinery are not just a source of aerodynamic losses but also a possible risk for the engines durability. Vannini et al. [5] stated that unsteady flows in seals can be a source of rotordynamic instability. Vance et al. [6] added that this is due to non-uniform pressure distribution around the seal. However, the source of non-uniformity is not defined. In turbomachinery, rotor eccentricity can be one source of non-uniformity. Furthermore, an excitation of the acoustic modes of the cavities can occur [5, 7]. As mentioned by multiple authors before, the ingress of hot main flow gas into the rim seal can damage the associated components of the engine [8, 9, 10]. Therefore, an accurate prediction of minimum purge flow rate $\dot{m}_{\text{purge}}$ is mandatory. The amount of ingress has been dramatically underestimated by steady state numerical simulations in the past, especially for low purge flow rates [11]. Slight improvements of the prediction of ingress has been achieved by time-resolved numerical simulations with small circumferential domains (one blade/vane passage). However, the ingress is significantly influenced by large scale unsteady flow features in the hub cavity, referred to as cavity modes [8, 9, 10]. Substantial improvements in the prediction of purge flow rates and ingress [12], as well as in the prediction of flow interaction between cavity flow and main flow [13] has been achieved by 360°-CFD domains. Comparison of numerical and experimental results shows that these CFD models are able to capture the right frequency of the cavity modes [12, 14]. However, there are still discrepancies between URANS and experimental results. It is assumed that these are related to turbulence modeling issues in modern RANS methods [15]. These can be reduced by use of scale-resolving simulations, such as large eddy simulation (LES). Since this numerical method is expensive in terms of computational resources, the computational domain needs to be as small as possible while also be able to capture the largest scales of the flow. An estimate of the largest scales, depending on design parameters or operating conditions is not known yet and is the objective of the present work in preparation of future LES.

EXPECTED UNSTEADY FLOWS IN THE LABYRINTH SEAL

Possible parameters influencing the periodicity of the largest scales in the flow will be selected based on a literature review of similar test cases with plain cavities, shroud labyrinth seals, and rim seals. In 1986 Gharib and Roshko [16] investigated the effect of flow oscillations on cavity drag for an axis-symmetric cavity with non-rotating walls. Additionally, no throttling (radial clearance) in front of the cavity exists in their experiments. They found that the boundary layer detaches at the backward-facing step, and rolls up into periodic vortices. These vortices are convected downstream, impinge on the forward-facing step, and are reflected as acoustic waves. Similar observations have been reported for rectangular cavities [17]. Gharib and Roshko found that the frequency f of flow oscillation strongly depends on the length of the cavity l, specifically from the ratio of the cavity length to the boundary layer thickness: l/δ_{b}. The frequency decreases with increasing l, increases for $l \geq l_{\text{crit}}$ and decreases again. They defined the Strouhal-Number St

$$\text{St} = f\frac{l}{V_\infty} \tag{1}$$

based on the cavity length l and the free stream velocity V_∞. These cavity modes typically have Strouhal-Numbers of $\text{St} = 1, 2, \ldots$. Similar to the flow separation at the backward-facing step in the experiments of [16], the flow in a labyrinth seal detaches at the leading edge of the sealing fin. This flow separation is not stable, rather it is pulsating with a distinct frequency, too. It is not clear yet if Eq. 1 can be used to estimate the vortex shedding frequency at the leading edge of a sealing fin. Nevertheless, Eq. 1 yields a frequency range of $3-15\,\text{kHz}$ for the first cavity mode ($\text{St} = 1$) of the stepped labyrinth seal considered here, depending on the definition of V_∞. From previous simulations it is known that this vortex shedding is non-uniform in the circumferential direction. The periodicity is not yet known, and is expected to be in a range of $10-20°$.

In the cavity between two adjacent sealing fins, a large vortex is driven by the leakage jet in axial direction, referred to as the cavity vortex. Depending on the pre-swirl parameter K, the cavity vortex can also have a circumferential velocity component. The pre-swirl parameter $K = V_\Theta/U$ is defined as the

ratio of the circumferential velocity of the fluid V_Θ and circumferential velocity of the rotor $U = \Omega \cdot R$. In addition, this vortex is sheared by the rotation of the inner or outer cylinder which results into a three-dimensional vortex structure and forms a spiral in the circumferential direction. Based on previous simulations with a 90° CFD domain, the periodicity of this vortex is expected in a range of $10-20°$.

Extensive work has been done in the analysis of cavity modes for rim seals in axial turbines. Jakoby et al. [18] investigated a 1.5-Stage turbine with rim seals. They found periodic flow structures inside the cavity decoupled from the rotor frequency and its harmonics, for example the rotor blade passing frequency (*RBPF*). The investigated range of dimensionless cooling flow rates C_W, defined as

$$C_W = \frac{\dot{m}_{\text{purge}}}{\mu \cdot R}, \tag{2}$$

was $0-25 \cdot 10^3$. In Eq. 2 $\dot{m}_{\text{purge}}$ is the leakage mass flow rate, μ the dynamic viscosity and R the radius of the rotor. For $C_W = 7 \cdot 10^3$, a cavity mode with a periodicity of 120° develops in the cavity of the rim seal which rotates with $0.8 \cdot \Omega$ in the direction of rotation (abs. frame of reference). The periodicity changes with C_W, until it is totally suppressed for $C_W \geq 15 \cdot 10^3$. Boudet et al. [11] achieved similar results for a one stage axial turbine with rim seals. They found cavity modes with a periodicity of 13.8°, and assumed the source of the cavity modes to be of the Taylor-Couette flow type. The frequencies associated to the cavity modes could be measured in the main flow path, which shows the significance of this effect. Again, the cavity modes were suppressed for C_W above a certain limit.

More recently, Schädler et al.[8] performed time-resolved experimental measurements in a 1.5-Stage high pressure turbine with rim seals. They also found the frequency of the cavity modes depend on C_W, and measured a periodicity of 45° for zero purge flow and 16.4° for intermediate purge flow. Schädler et al. also mentioned that the frequency of the cavity modes are within the human perception of sound, thus increasing the noise level up to 18 dB. This enforces the relevance of cavity modes for the turbomachinery design process.

The work of Beard et al. [9], Cao et al. [12], and Boudet et al. [19] show that the cavity modes in rim seals are not caused by turbine blades or vanes, because their experimental measurements were obtained without blades and vanes. Cao et al. [12] investigated the rim seal of an Alstom two-stage high pressure axial turbine. Numerical and experimental results confirm the presence of cavity modes with a periodicity of $18-30°$ in the circumferential direction . The investigation was performed for a dimensionless cooling flow rate of $C_W = 5.9 \cdot 10^3$. Boudet et al. [19] studied different rim seal designs with 360° URANS simulations. In the Gnome H1200 Power Turbine Module, they found cavity modes with a periodicity of 6.4° for a dimensionless cooling flow rate $C_W = 5.9 \cdot 10^3$. Beard et al. [9] found cavity modes with a periodicity of $12.4-13.8°$. They found the cavity modes to be almost independent from the rotational speed N, and a the dimensionless cooling flow rate in a range of $7000-9000$ rpm and $C_W = 0-3.5 \cdot 10^3$. This is not in accordance with the conclusions of others how identified a dependency of the cavity modes from C_W.

Rebholz et al. [20] experimentally validated low frequency oscillation in the shroud cavity of a 1.5-stage low pressure turbine of around 10% blade passing frequency. Suppressing this low frequency oscillation results in a 12 dB reduction of noise, but a 0.7% drop of total-total stage efficiency. However, they where not able to capture these oscillations with 360° URANS domains. This might be caused by the $k-\omega$ turbulence model, which produces high eddy viscosity in the core of the cavity vortex and suppresses unsteady effects [21]. Furthermore, the periodicity of this mode is not mentioned in [20].

To conclude this review, the periodicity of the largest scales is expected to be in a range of $6-120°$ in the circumferential direction, and seems to depend mainly on the mass flow rate. For a given geometry of the seal, the leakage rate is driven by the seal pressure ratio, the pre-swirl angle of the flow, and the rotational speed of the rotor. These parameters will therefore be varied in this study. Table 1 summarizes the different cases investigated here.

Table 1 Definition of the Investigated Cases

Case	π/π_{ref}	N in min^{-1}	K_{Inlet}
Ref	1	6000	0.3
V1	**1.05**	6000	0.3
V2	**0.95**	6000	0.3
V3	1	**3000**	0.3
V4	1	**0**	0.3
V5	1	6000	**0**

EXPERIMENTAL SETUP

The case investigated in the present paper is part of an experimental investigation of stepped labyrinth seals by Denecke et al. [22] and others [23, 24]. Detailed information is given in [22]. Figure 1 shows a sketch of the rig. The seal has a rotating hub with four sealing fins, and a stationary casing. While the rig allows two flow directions to be investigated, only the divergent flow direction will be investigated here. The design is equivalent to the seal investigated by Mahle and Schmierer [25], which is a labyrinth seal typically found in aero engine low-pressure turbines. The seal has a clearance-to-fin height ratio of $c/h = 0.325$ and the cavity length-to-fin height ratio is $l/h = 2$. The rig can operate at different pressure ratios, i.e. leakage rates. However, LDV measurements have only been published

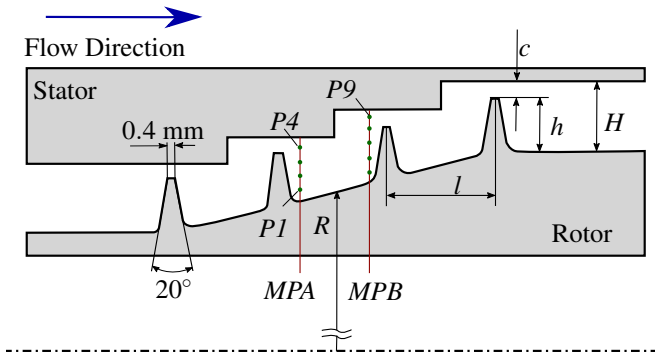

Figure 1 Stepped Labyrinth Seal Investigated Experimentally by [22]. LDV Measurements are Available for the Green Points *P1-P9* at Measurement Plane *MPA* and *MPB*

for one operating point with an axial Reynolds-Number of $\mathrm{Re}_{\mathrm{ax}} = 10000$, defined as

$$\mathrm{Re}_{\mathrm{ax}} = \frac{\dot{m}}{\mu \cdot \pi \cdot R}. \tag{3}$$

In Eq. 3, $\dot{m}$ is the leakage mass flow rate, μ the dynamic viscosity, $\pi = {p_{\mathrm{tot,Inlet}}}/{p_{\mathrm{stat,Outlet}}}$ the pressure ratio, and $R = 0.253$ m the rotor mean radius. The rotational speed of the rotor is 6000 rpm, and the flow enters the cavity with a swirl ratio of $K = 0.3$. This case was already used in [21] to evaluate different numerical setups in terms of turbulence modeling and spatial discretization techniques. Unfortunately, time-resolved measurements have not been published until now. The time-resolved computational results presented here therefore can not be validated directly. The validation is limited to a comparison with time-averaged results.

Calculating the dimensionless cooling flow rate with the intermediate seal radius R gives $\mathrm{C_W} = 16150$. According to Jakoby et al. [18] and Boudet et al. [11], this operating point is on the upper limit where cavity modes have been observed in turbine rim seals. The vortex-shedding frequency (Eq. 1) is $f = 10600$ Hz with V_∞ being the time and spatially-averaged absolute velocity or $f = 3470$ Hz, with V_∞ being the time and spatially-averaged axial velocity in the second clearance. Yet, it is not clear how to define V_∞ to appropriately predict the vortex shedding frequency. Anyway, the expected range of frequencies is within the human perception of sound.

NUMERICAL SETUP

The investigations will be carried out using the commercial flow solver ANSYS-CFX 18.2. At the inlet of the domain radial profiles of the total pressure, the total temperature, and the three dimensional flow vector was specified. Since no measurements of the inlet turbulence are available, the turbulence intensity at the inlet was set to 5 % and a length scale of $1.11 \cdot 10^{-4}$m was assumed. The inlet turbulence is expected to be of minor relevance, since the acceleration in the first tip clearance will damp most of the inlet turbulence. The boundary layers are assumed to be fully turbulent, i.e. transitional affects are neglected. At the outlet, a static pressure was defined.

The scale-adaptive shear stress transport turbulence model (referred to as SST-SAS) will be used to account for turbulence in the seal. The SST model proposed by Menter [26], is based on the $k-\omega$ model and blends to the $k-\varepsilon$ model in the free stream. Moreover, the SST turbulence model accounts for the Bradshaw-Assumption, that the Reynolds-Stresses are proportional to the turbulent kinetic energy ($\overline{u_i' u_j'} \sim k$) in boundary layer flows. Thus, the eddy viscosity ν_t is given by

$$\nu_\mathrm{t} = \frac{a_1 k}{\max\left(a_1 \omega, S F_2\right)} \tag{4}$$

close to the wall [26]. In Eq. (4) a_1 refers to a model constant, ω to the specific turbulent dissipation rate, S to the vorticity, and F_2 to a blending function that restricts Eq. (4) to the wall. In [21], it was shown that the Bradshaw-Limiter is the main reason why the model is able to resolve the transient nature of the cavity flow while the $k-\omega$ [27]model fails to do so.

The SAS extension of the SST model allows the model to resolve even more turbulent scales of the flow. According to Fröhlich and von Terzi [28], this is achieved by introducing the von Karman length scale l_{vk} into the ω-equation via a source term. When the model captures large scale unsteadiness, l_{vK} decreases and the source term F_{SAS} increases. So, ω increases and the eddy viscosity is reduced. As a consequence, the model adjusts to already resolved scales and avoids the damping of classical RANS turbulence models [29].

During this study, it was noticed that the pure SST model was not able to resolve the time varying flow field anytime, especially for cases with low sealing mass flow rates. Therefore, the SST-SAS model was selected here. However, as shown by [21], the computational effort is much larger (due to CFL-Number constraints) and needs careful validation.

A bounded central difference scheme was selected as the advection scheme. This scheme is blending from a central difference in unsteady flow regions to a second order upwind scheme in steady flow regions. A second-order Backward Euler time discretization technique was used for unsteady simulations. The CFL-Number has been limited to $\mathrm{CFL} \leq 1$.

Domain and Spatial Discretization

To avoid the influence of periodic boundary conditions on the prediction of circumferential cavity modes, the whole annulus of the labyrinth seals will be simulated. Therefore, the expected computational effort to conduct this study is tremendous. To achieve an appropriate compromise between accuracy and computational effort, the computational domain as it was

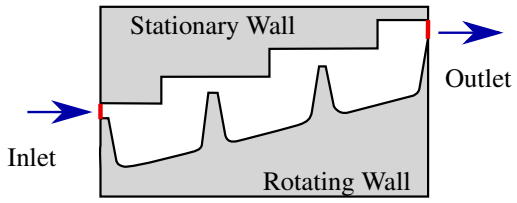

Figure 2 Computational Domain for the Simulations

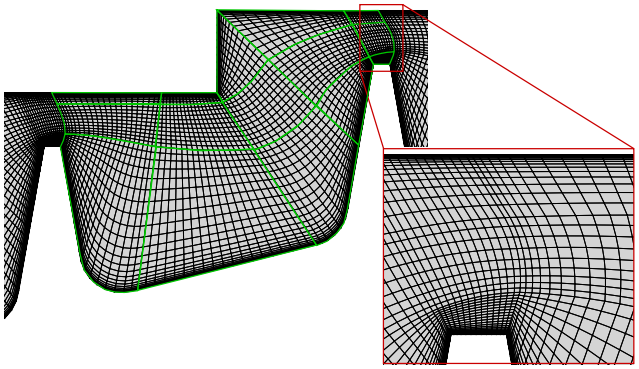

Figure 3 Blocking Structure with Stream Aligned Mesh. Only the Second Cavity is Shown.

used in [21] was narrowed, i.e. the inlet and outlet sections have been removed. As can be seen in Fig. 2, the inlet is placed at the leading edge of the first sealing fin and the outlet at the leading edge of the last sealing fin. This way, both panels have an attached flow which should improve convergence.

As it was shown by Zaib et al. [30] and Wein et al. [21], substantial improvements in the stability and accuracy of the results can be achieved when the computational grid is aligned to the local flow vector. The alignment reduces numerical diffusion, and therefore improves the accuracy. Therefore, such a grid has been used here. The intermediate grid reported in [21] was selected to ensure reasonable prediction of the cavity vortex [21]. The non-dimensional wall distances are $x^+ \leq 50$, $y^+ \leq 1$ and $\theta^+ \leq 200$ given by $x_i^+ = \Delta x_i u_\tau / \nu$. The cell size increases with a factor of 1.2 in wall normal direction.

A grid sensitivity study was conducted in [21], where the grid has been refined twice by a factor of two ($r_{12} = r_{23} = 1/2$) in all spatial dimensions. As reported in [21], the estimated extrapolated relative error (*EERE*) according to Roache [31] of the computational grid used here is 1.0% for the prediction of the leakage mass flow rate. This error is acceptable, and presumably within the uncertainty of the measurements.

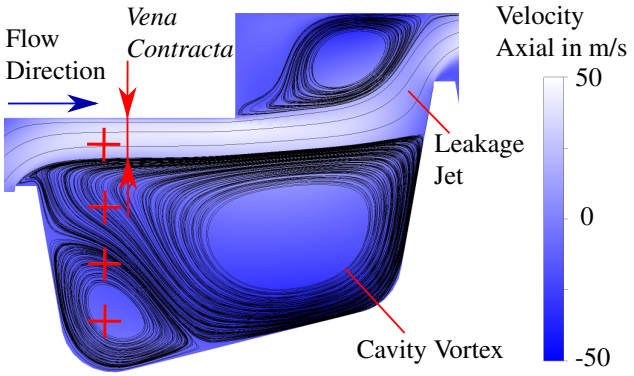

Figure 4 Flow Field in the Second Cavity of the Seal.

RESULTS

Flow Field

Figure 4 shows an overview of the average flow field in the second cavity of the seal. The flow is dominated by the large cavity vortex, which is driven by the leakage jet in axial direction and sheared by the rotation of the rotor in the circumferential direction. The leakage jet detaches at the leading edge of every fin, and forms a *vena contracta* downstream. Furthermore, three additional smaller vortices can be seen downstream of the sealing fin and the backward facing step at the shroud.

Validation

In order to validate the computational setup the results will be compared with measurements obtained by Denecke et al. [22]. Since only time-averaged results of the velocity components at two axial locations in the second vortex chamber (see Fig. 1) have been published, the validation is limited to time-averaged results. Time-averaging in CFD was performed for at least one revolution of the rotor. The strength of the cavity vortex is given by the skewness of the axial velocity profile. As can be seen in Fig. 5, the cavity vortex is slightly under predicted. This is in agreement with the prediction in [15] and [21]. In contrast, the prediction of the swirl velocity given by the normalized circumferential velocity component in Fig. 5 is over predicted. So, the acceleration of the fluid in the circumferential direction by viscous friction on the rotor surface is over predicted (referred to as drag effect). In comparison to the results presented in [15] and [21], the prediction of swirl development is worse. It is expected that this is due to wrong boundary conditions at the inlet of the computational domain. Shifting the results by a normalized swirl of -0.175 gives reasonable agreement with the experimental results. Since the prediction of the correct velocity field in the cavity is not the primary aim of this work, the error in the boundary conditions is considered to be acceptable. It is therefore expected that the accuracy of the computational model for the reference case of Denecke et al. [22] is appropriate.

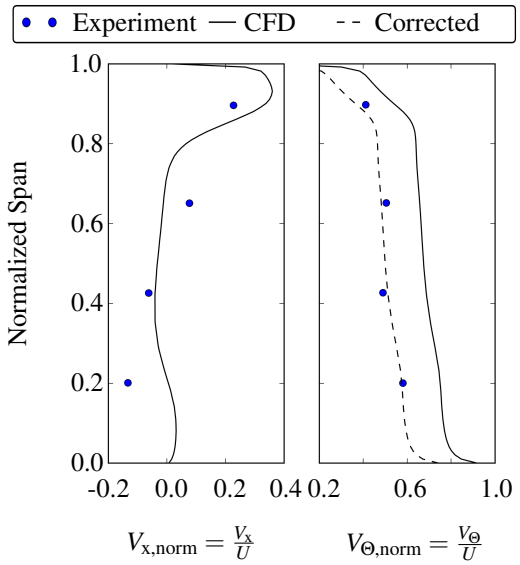

Figure 5 Normalized Axial and Swirl Velocity at *MPA*.

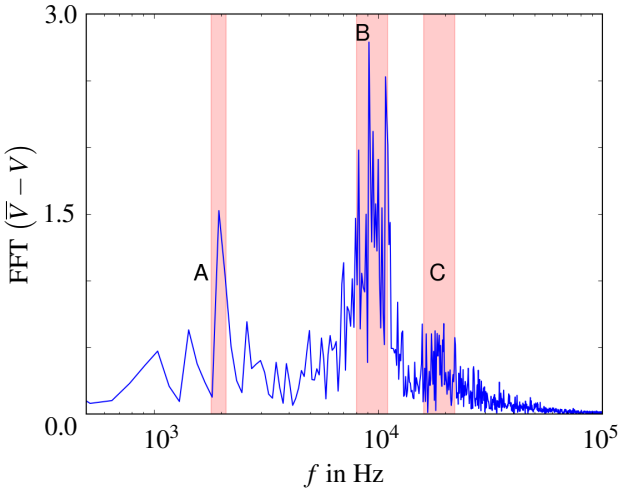

Figure 6 Frequency Spectrum at *P*4 for Reference Operating Point.

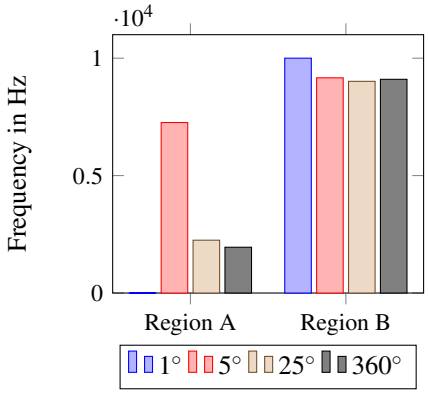

Figure 7 Dominant Frequencies in Region A and B Recorded at *P*4 for Different Sector Sizes.

Influence of CFD Sector Size on the Prediction of Unsteady Flows

The sensitivity of the results on periodic boundary conditions was investigated through time-resolved simulations with computational domains of different size in the circumferential direction. Starting with a sector of 1°, additional domains with 5°, 25°, and 360° have been investigated. Monitor points have been placed at $P1 - P4$, see Fig. 1, 4, and the velocity was recorded. An example of the resulting velocity spectrum is shown in Fig. 6 for the simulation of the full annulus, referred to as *reference case*. The spectrum is evaluated for *P*4. As already shown in [21], the velocity signal from the SST-SAS model contains much more fluctuations and frequencies, presumably due to its ability to resolve turbulence. The velocity signal from an URANS-SST simulation looks like a sinusoidal signal [21]. The spectrum has three pronounced regions; A) Low frequencies from 1900-2100 Hz, B) dominant frequencies in a range of 8000-11000 Hz, and C) high frequencies of low amplitude ranging from 16000-22000 Hz. Region C contains first harmonic frequencies of region B.

To demonstrate the influence of periodic boundary conditions on the solution, the two most dominant frequencies in Region A and B in the spectrum of each simulation are given in Fig. 7. The simulation with a periodic constraint of 1° resolves only four peaks in the whole velocity spectrum. The periodic constraint seems to suppress the resolution of turbulent scales. In region A, no frequency or time-depending effect is captured by this small domain. The predicted frequencies are up to 100% higher than for the reference case. With increasing sector size, the unsteadiness of the flow field increases. The prediction of the frequency with the highest amplitude in region B is in excellent agreement and below 1% difference, for all three domains above 1° periodicity. Thus, it is expected that the associated effect is not influenced by periodic boundary conditions anymore. However, the domains with 1° and 5° periodicity are not able to accurately predict the peak in region A. The domains with 25° and 360° periodicity are in good agreement. So, it is concluded that this frequency corresponds to circumferential modes in the cavity.

Classification of Frequencies

In order to identify the largest flow structure in the circumferential direction, the frequencies observed in Fig. 6 are associated to flow features in the labyrinth seal. Region B with a frequency of approximately 9000 Hz, belongs to vortex-shedding at the leading edge of the second sealing fin. Hence, this frequency is most pronounced at *P*4. The vortex-shedding is illustrated in Fig. 8 as a series of instantaneous vorticity fields in the cavity. The shear layer between the leakage jet and the cavity vortex is not stable, rather it moves up and down in the radial direction, referred to as leakage pulsation. Presumably, this is due to unbalanced aerodynamic forces in the clearance

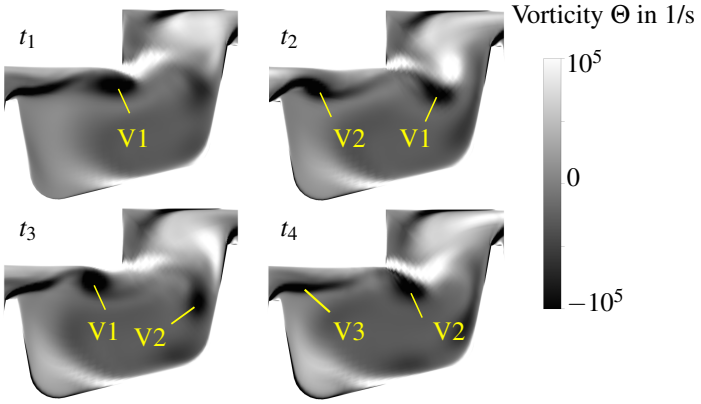

Figure 8 Vortex Shedding at the Fin of the Seal for Different Timesteps t_1-t_4, Colored by the Vorticity (Circumferential Component).

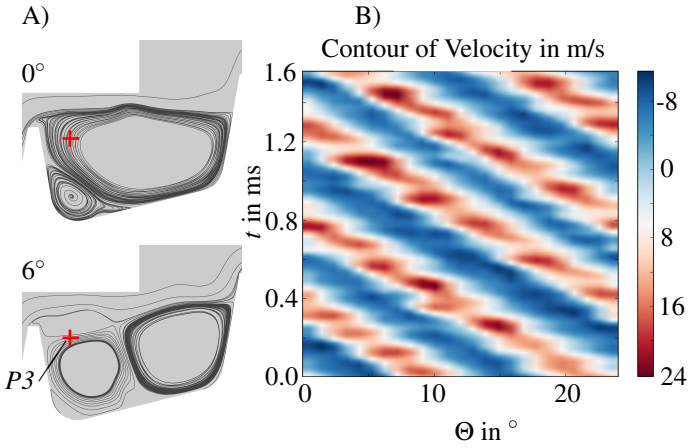

Figure 9 A: Circumferential Growth and Shrink of the Cavity Vortex. B: Space-Time Diagram of the Axial Velocity on a Circumferential Line of Radius $P3$.

between the casing and the fin. Here, the leakage jet has a strong momentum in the axial direction, however the cavity vortex pushes the leakage jet towards the casing. Consequently, the shear layer rolls up into single vortices V1, V2, and V3. These vortices are convected downstream by the leakage jet until they impinge onto the next fin. Here, they are stretched and sucked into the next clearance. The calculated frequency of this process is in agreement with the estimated range of frequencies from Eq. (1), depending on the definition of V_∞. The square root of the axial- and circumferential velocities, together with the length of a streamline from one fin to another gives an estimate for the lower limit of region B (f=8000 Hz) while the axial velocity together with the axial spacing of two fins gives an estimate for the upper limit of region B (f=10084 Hz). The fluctuation of total pressure caused by this vortex-shedding has amplitudes up to $\pm$1500 Pa, which is approximately half the fluctuation of total pressure caused by the wake of a stator in a low pressure turbine. This effect seems to be significant and may cause an instantaneous interaction with the main gas path of an engine. It could therefore be used to increase the momentum in the wake of a rotor, to reduce mixing loses, or wake-induced transition downstream.

Region A in the spectrum (Fig. 6) corresponds to a periodic growth and shrink of the cavity vortex. This growth and shrink does not happen simultaneously over the circumference. Figure 9, A) shows the instantaneous velocity field in the second cavity at 0° and 6° circumferential position. As can be seen, at 0° the cavity vortex occupies almost the whole cavity, while at 6° the cavity vortex is much smaller in the axial direction, for the same time step. This structure, referred to as *lobes* has a periodicity of approximately 12°, and the fluctuation of total pressure reaches $\pm$1000 Pa at $P3$. As already reported for turbine rim seals by multiple authors, these lobes are moving in the direction of rotation. For the reference case, the angular velocity of the lobes is 76% of disc speed, i.e. $0.76\Omega_{\text{Rotor}}$. In Fig. 9, this is illustrated as a space-time diagram of the velocity in the axial direction, evaluated for a line of radius $P3$. The red zones correspond to a situation where the cavity vortex has its smallest size in the axial direction. The fluctuations within the red or blue regions are due to the leakage pulsation (Region B in the spectrum).

These lobes are the largest scales in the circumferential direction, i.e. they define the required size of the computational domain. The error from using a domain of 25° is slight in comparison to the savings of computational resources. Regardless, these large scales make the computation of cavity flows with scale-resolving methods, like Large Eddy Simulation (LES) rather expansive.

Dependence on Operating Conditions

Numerous experimental investigations report a dependence on operating conditions, such as C_W or N. The frequencies associated with leakage pulsation, and the lobes are summarized in Fig. 10. The results from the simulations without pre-swirl of the flow (V5 in Tab. 1) and with a reduced pressure ratio (V2 in Tab. 1) show only few frequencies in the velocity spectrum. Both cases do not resolve the lobes, only the leakage pulsation with frequencies of 12400 Hz for case V5, and 8200 Hz for case V2. Again, this is in accordance to Eq. 1. Reducing the seal pressure ratio reduces the leakage mass flow rate and therefore V_∞. Reducing the pre-swirl of the flow increases the leakage mass flow rate and therefore V_∞. Due to the higher leakage mass flow rate, $C_W > 18000$ and the lobes are suppressed. In context of C_W, it is not clear why the lobes are suppressed for case V2 with reduced seal pressure ratio. For this case, $C_W = 9540$. One observation is that the leakage pulsation is much weaker in comparison to the reference case. Assuming that the leakage pulsation causes the lobes, i.e. the periodic growth and shrink of the cavity vortex to establish it might be an explanation for the fact that they are not present in the solution.

As can be seen in Fig. 10, the frequency associated to leakage pulsation decreases to 8500 Hz and the frequency of

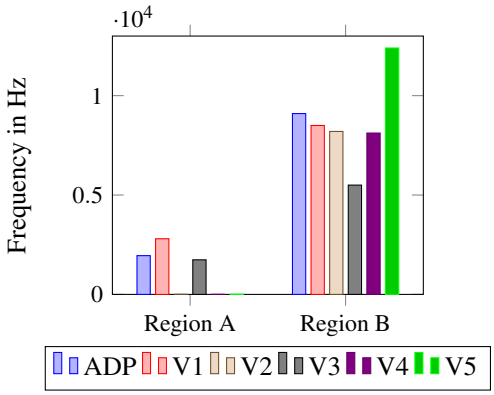

Figure 10 Dominant Frequencies in Region A and B Recorded at $P4$ for Different Operating Conditions.

the lobes increases to 2800 Hz, when the seal pressure ratio is increased (V1). However, the periodicity of the lobes does not change. Yet, they are moving in the direction of rotation with $0.93\Omega_{\text{Rotor}}$. Since the C_W of this operating point is $C_W = 20400$, the dimensionless cooling flow rate does not seem to be useful to estimate the presence of lobes in stepped labyrinth seals.

Reducing the rotational speed to $3000rpm$ (V3), reduces the frequency of the leakage pulsation by 40% in comparison to the ADP. However, the spectrum of this case is not entirely converged. This simulation will be continued to stabilize the statistics. Without a rotation of the rotor (V4) the lobes are almost not present in the solution. The frequency associated to leakage pulsation is 8120 Hz. The space-time diagram (not shown here) of this case does not show the lobes as largest scales in the cavity but the leakage pulsation with a size of approximately 6.43°.

CONCLUSIONS

It has been shown that the size of the computational domain can have a significant influence on the prediction of the time-resolved flow field in the cavities of a stepped labyrinth seal. High frequencies are due to leakage pulsation and low frequencies are due to large coherent flow structures, so called lobes, which extend over 12° in circumferential direction. The latter determine the required size of the CFD domain for scale-resolving simulations. The lobes are moving in the direction of rotation. If the CFD domain is too small in circumferential direction, the lobes cannot be resolved and the frequency of leakage pulsation is overpredicted. This can be critical if the CFD model is used to investigate the time-resolved interaction of the leakage flow with the core flow of turbomachinery.

The influence of operating conditions on the time-resolved flow in the cavities has been investigated through the parameter variation of rotational speed, pre-swirl, and seal pressure ratio. While leakage pulsation is present for all investigated cases, the presence and frequency of the lobes varies with the pre-swirl angle and the seal pressure ratio. The periodicity of the lobes does not change with the seal pressure ratio, rather their frequency. The dependence of the lobes on the dimensionless cooling flow rate is contrary to what has been observed for turbine rim seals. More work must be done to work out correlations for the frequency and the size of the lobes. However, the expected range of frequencies for the leakage pulsation can be estimated based on a length scale and a velocity scale. This is useful when estimating the required time step for unsteady simulations with URANS turbulence models. Currently, there is no valid correlation to estimate the periodicity of the lobes. Based on the present study, the authors recommend performing URANS simulations with full annulus CFD models to identify the required size of the computational domain for LES.

Future work will investigate different operating conditions as well as different designs of the seal to develop correlations for the periodicity and the frequency of the lobes and to improve the estimate for the leakage pulsation frequency. Furthermore, scale-resolving simulations will be performed to investigate the poor prediction of the velocity profiles with URANS turbulence models presented here.

ACKNOWLEDGMENTS

The authors gratefully thank ANSYS for providing CFX in an academic license. Furthermore, the authors thank the Leibniz Universität Hannover (LUIS) and the North-German Supercomputing Alliance (HLRN) for their provision of computational resources. The investigations were conducted as part of the joint research program COOREFLEX-Turbo 4.2.5a in the frame of AG Turbo. It was supported by the Bundesministerium für Wirtschaft und Technologie (BMWi) and MTU Aero Engines AG.

REFERENCES

[1] Cumpsty, N., 2010. "Preparing for the Future: Reducing Gas Turbine Environmental Impact: GT2010-22729". Vol. 132 of *Journal of Turbomachinery*.

[2] Biester, M. H.-O., Henke, M., Guendogdu, Y., Engel, K., and Seume, J. R., 2011. "Unsteady Blade-Wake Interaction: A Correlation Between Surface Pressure Fluctuations and Loss Generation: GT-2011-69616". ASME Conference Proceedings, 2011.

[3] Henke, M., Wein, L., Kluge, T., Guendogdu, Y., Biester, M., and Seume, J., R., 2016. "Experimental and Numerical Verification of the Core-Flow in a New Low-Pressure Turbine: GT2016-5710". Turbo Expo: Power for Land, Sea, and Air.

[4] Giboni, A., Wolter, K., Menter, J. R., and Pfost, H., 2004. "Experimental and Numerical Investigation Into the Unsteady Interaction of Labyrinth Seal Leakage Flow and Main Flow in a 1.5-Stage Axial Turbine: GT-2004-53024". ASME Turbo Expo 2004.

[5] Vannini, G., Thorat, M. R., Childs, D. W., and Libraschi, M., 2010. "Impact of Frequency Dependence of Gas Labyrinth Seal Rotordynamic Coefficients on Centrifugal

Compressor Stability: GT2010-22039". Turbo Expo: Power for Land, Sea, and Air.

[6] Vance, J. M., Zeidan, F. Y., and Murphy, B., 2010. "Machinery Vibration and Rotordynamics".

[7] di Mare, L., Imregun, M., Green, J. S., and Sayma, A. I., 2010. "A numerical study of labyrinth seal flutter". *Journal of Tribology,* ***132***.

[8] Schaedler, R., Kalfas, A. I., Abhari, R. S., Schmid, G., and Voelker, S., 2017. "Modulation and radial migration of turbine hub cavity modes by the rim seal purge flow". *Journal of Turbomachinery,* ***139***.

[9] Beard, P. F., Gao, F., Chana, K. S., and John, C., 2017. "Unsteady Flow Phenomena in Turbine Rim Seals". *Journal of Engineering for Gas Turbines and Power*.

[10] Wang, C.-Z., Mathiyalagan, S. P., Johnson, B. V., Glahn, J. A., and Cloud, D. F., 2014. "Rim seal ingestion in a turbine stage from 360 degree time dependent numerical simulation". *Journal of Turbomachinery,* ***136***.

[11] Boudet, J., Hills, N. J., and Chew, J. W., 2006. "Numerical Simulation of the Flow Interaction Between Turbine Main Annulus and Disc Cavities: GT2006-90307". Proceedings of ASME Turbo Expo 2006.

[12] Cao, C., Chew, J. W., Millington, P. R., and Hogg, S. I., 2004. "Interaction of Rim Seal and Annulus Flows in an Axial Flow Turbine". *J. Eng. Gas Turbines Power,* ***126***, pp. 786–793.

[13] Schuepbach, R., Abhari, R. S., Rose, M. G., Germain, T., Raab, I., and Gier, J., 2008. "Effects of Suction and Injection Purge-Flow on the Secondary Flow Structures of a High-Work Turbine: GT2008-50471". Proceedings of ASME Turbo Expo 2008.

[14] O'Mahoney, T., Hills, N., and Chew, J., 2012. "Sensitivity of les results from turbine rim seals to changes in grid resolution and sector size". *Progress in Aerospace Sciences,* ***52***, pp. 48–55.

[15] Tyacke, J., Jefferson-Loveday, R., and Tucker, P., 2012. "On LES Methods Apllied to Seal Geometries: GT-2012-68840". ASME Turbo Expo 2012.

[16] Gharib, M., and Roshko, A., 1986. "The effect of flow oscillation on cavity drag". *Journal of Fluid Mechanics,* ***177***, pp. 501–530.

[17] Rossiter, J. E., 1964. "Wind-Tunnel Experiments on the Flow over Rectangular Cavities at Subsonic and Transonic Speeds". Aeronautical Research Council Reports and Memoranda.

[18] Jakoby, R., Zierer, T., Lindblad, K., Larsson, J., deVito, L., Bohn, D. E., Funcke, J., and Decker, A., 2004. "Numerical Simulation of the Unsteady Flow Field in an Axial Gas Turbine Rim Seal Configuration: GT-2004-53829". ASME Turbo Expo 2004.

[19] Boudet, J., Autef, V. N. D., Chew, J. W., Hills, N. J., and Gentilhomme, O., 2004. "Numerical Simulation of Rim Seal Flows in Axial Turbines". RAeS Aerospace Aerodynamics Research Conference.

[20] Rebholz, P. S., Krebietke, S., Abhari, R. S., and Kalfas, A. I., 2016. "Turbine aerodynamic low-frequency oscillation and noise reduction using partial shrouds". *Journal of Propulsion and Power,* ***32***.

[21] Wein, L., Seume, J. R., and Herbst, F., 2017. "Improved Prediction of Labyrinth Seal Performance Through Scale Adaptive Simulation and Stream Aligned Grids: GT2017-64257". Proceedings of ASME Turbo Expo 2017.

[22] Denecke, J., Dullenkopf, K., Wittig, S., and Bauer, H.-J., 2005. "Experimental Investigation of the Total Temperature Increase and Swirl Development in Rotating Labyrinth Seals: GT-2005-68677". ASME Turbo Expo 2005.

[23] Willenborg, K., Kim, S., and Wittig, S., 2001. "Effects of Reynolds Number and Pressure Ratio on Leakage Loss and Heat Transfer in a Stepped Labyrinth Seal: GT-2001-0123". Proceedings of ASME Turbo Expo, 2001.

[24] Schramm, V., Denecke, J., and Kim, S.and Wittig, S., 2004. "Shape Optimization of a Labyrinth Seal Applying the Simulated Annealing Method". International Journal of Rotating Machinery, 10(5):365-371, 2004.

[25] Mahle, I., and Schmierer, R., 2011. "Inverse Fin Arrangement in a Low Pressure Turbine to Impprove the Interaction Between Shroud Leakage Flow and Main Flow: GT-2011-45250". ASME Turbo Expo 2011.

[26] Menter, F. R., 1994. "Two-Equation Eddy-Viscosity Turbulence Models for Engineering Applications". *AIAA Journal, Vol. 32, No. 8 (1994), pp. 1598-1605*.

[27] Wilcox, D. C., 1998. *Turbulence Modelling for CFD*, 2 ed. DCW Industries, Inc.

[28] Froehlich, J., and von Terzi, D., 2008. "Hybrid LES RANS Methods for the Simulation of Turbulent Flows". pp. 349–377.

[29] Menter, F. R., 2009. "Review of the Shear-Stress Transport Turbulence Model Experience From an Industrial Perspective". *International Journal of Computational Fluid Dynamics,* ***23***(4), pp. 305–316.

[30] Zaib, A., and Tucker, P. G., 2013. "Multiblock Structured Mesh Generation for Turbomachinery Flows". Proceedings of the 22nd International Meshing Roundtable, Springer International.

[31] Roache, P. J., 1994. *Perspective A Method for Uniform Reporting of Grid Refinement Studies*. Journal of Fluids Engineering, September.